ELSEVIER

Contents lists available at ScienceDirect

### Toxicology in Vitro

journal homepage: www.elsevier.com/locate/toxinvit



## Mechanisms of the immune response cause by cationic and anionic surface functionalized cellulose nanocrystals using cell-based assays



Hannah W. Despres<sup>a</sup>, Adham Sabra<sup>a</sup>, Phil Anderson<sup>a</sup>, Usha D. Hemraz<sup>b</sup>, Yaman Boluk<sup>c</sup>, Rajesh Sunasee<sup>a,\*\*</sup>, Karina Ckless<sup>a,\*</sup>

- <sup>a</sup> Department of Chemistry, State University of New York at Plattsburgh, Plattsburgh, NY 12901, USA
- <sup>b</sup> National Research Council, Montreal, Quebec, Canada
- <sup>c</sup> Department of Civil & Environmental Engineering, University of Alberta and National Institute for Nanotechnology, National Research Council, Edmonton, Alberta, Canada

#### ARTICLE INFO

# Keywords: Cellulose nanocrystals Surface charge Nanomaterials Immunogenicity Reactive oxygen species NLRP3 inflammasome

#### ABSTRACT

The interest in functionalized cellulose nanocrystals (CNCs) for multiple biomedical application has been increasing in recent years. CNCs are suitable to functionalization with an array of polymers, generating chemically related nanomaterials with different morphologies, surface charges that can affect bioreactivity, including immune response. In this study, we sought to understand the mechanistic differences regarding immunological responses evoked by functionalized CNCs and whether surface charges play a role in this effect. We investigated the effect of a cationic, CNCs-poly(APMA), and an anionic, CNCs-poly(NIPAAm) derivatives on the secretion of inflammatory cytokines, mitochondria-derived ROS and mitochondrial function and antioxidant response as well as on endoplasmic reticulum (ER) stress, in human and murine inflammatory cells. The cationic CNCs-poly (APMA) evoked a more robust immunological response in murine cell line, while the anionic CNCs-poly (NIPAAm) showed a significant NLRP3 inflammasome-dependent and independent immunological response in human monocytes. Moreover, CNCs-poly(NIPAAm) induced greater formation of acidic vesicular organelles, mitochondrial ROS in non-stimulated cells while CNCs-poly(APMA) mainly affected mitochondrial function by decreasing the intracellular ATP. The differences on the biological responses may be related to the surface charges of CNCs, and their likely interactions with intra and extracellular biomolecules.

#### 1. Background

Cellulose, the most abundant carbon-based polymer on the earth, has a long history of use in the pharmaceutical industry because of its excellent compaction properties when blended with other pharmaceutical excipients, making it suitable as a filler in tablets for oral administration of drugs Kalia et al., 2011. Recently, cellulose nanocrystals (CNCs), which can be obtained from the acid hydrolysis of native

cellulose, have emerged as a new class of renewable nanomaterial for multiple biomedical applications, from drug and gene delivery systems to tissue scaffolding. These rigid "rod-like" cellulose crystals typically display a diameter of 5–50 nm and a variable length from 100 to 500 nm. CNCs possess remarkable strength and physicochemical properties with several potential applications. In addition, the presence of ample reactive hydroxyl groups on the surface allows diverse chemical functionalization (Habibi et al., 2010). The degree of functionalization

Abbreviations: CNCs, Cellulose nanocrystals; NFC, nanofibrillated cellulose; NPs, nanoparticles; CNCs-poly(APMA), CNCs-poly(N-3-aminopropylmethacrylamide); CNCs-poly(NIPAAm), CNCs-poly(N-isopropylacrylamide); (CNCs-poly(N-aminoethylmethacrylamide), CNCs-poly(AEMA2); NLRP3, apoptosis-associated speck-like protein containing a CARD; ELISA, enzyme-linked immuno assay; IL-1β, Interleukin 1beta; TNF-α, tumor necrosis factor alpha; UPR, unfolded protein response; ATP, adenosine triphosphate; AO, acridine orange; DAPI, 4′,6-diamidino-2-phenylindole; LPS, lipopolysaccharide; PMA, phorbol myristate acetate; MSU, monosodium urate; BSA, bovine serum albumin; LSM, Lymphocyte separation medium; SOD, superoxide dismutase; Trx2, thioredoxin 2; Prx1, peroxiredoxin 1; PrxSO3, oxidized peroxiredoxins; NF-κB, nuclear factor kappa B; LC3B, autophagy-related protein LC3 B; ATG13, autophagy-related protein 13; PDI, protein disulfide isomerase; TMB, 3,3′,5,5′-tetramethylbenzidine; ECL, Enhanced chemiluminescence substrate; ROS, reactive oxygen species; SDS-PAGE, sodium dodecyl sulfate polyacrylamide gel; PBMCs, peripheral blood mononuclear cells; ER, endoplasmic reticulum

<sup>\*</sup> Correspondence to: K. Ckless, Department of Chemistry, State University of New York at Plattsburgh, Hudson Hall, Room 231, 101 Broad Street, Plattsburgh, NY, USA.

<sup>\*\*</sup> Correspondence to: R. Sunasee, Hudson Hall, Room 223, 101 Broad Street, Plattsburgh, NY, USA. E-mail addresses: rsuna001@plattsburgh.edu (R. Sunasee), kckle001@plattsburgh.edu (K. Ckless).

and the nature of the functional groups impact the charge density and therefore the physical-chemical properties of these nanomaterials (Endes et al., 2016). Moreover, while these chemical functionalization methods can generate a wide variety of surface modified CNCs for multiple biomedical applications, they also extend the possibility of these nanomaterials to interact with biomolecules causing an array of biological activities (Endes et al., 2016; Johnston et al., 2012). One of the important emerging aspects of the nanoparticle-cell interactions in biological systems is the potential for nanoparticles to evoke an immune/inflammatory response Dobrovolskaia, 2015. It is well-known that some nanomaterials Lunov et al., 2011, especially those having a "needle-like" morphology can evoke an inflammatory/immunological response in mammalian cells by inducing the secretion of the inflammatory cytokine interleukin-1β (IL-1β) (Sunasee et al., 2015; Franchi et al., 2009). In general, assessing biological effects of nanomaterials including cytotoxicity and immunogenicity can be challenging due to the diversity in sizes, morphology, coatings, and surface reactivities. In a recent study, the immunogenicity of two different cellulose-based nanomaterials, CNCs and nanofibrillated cellulose (NFC), were investigated. Interestingly, CNCs caused an inflammatory response with significantly elevated inflammatory cytokines/chemokines compared to NFC. In addition, the study suggested that CNC particles, and not NFC, were taken up by the cells (Menas et al., 2017). It is clear now that the extent of the response among different nanomaterials and the mechanisms by which they evoked this immunological response is not totally understood, but it appears to involve alterations in the production of reactive oxygen species (ROS) by mitochondria and endoplasmic reticulum (ER) stress Cao et al., 2017.

While a number of recent studies have shown that surface cationization of CNCs could provide functional cationic CNCs for potential biomedical applications (Sunasee et al., 2016; Sunasee and Hemraz, 2018), the biological responses of cationic CNCs are not well studied. Previously, we reported that a cationic CNCs derivative (CNCs-poly(N-aminoethylmethacrylamide), (CNC-AEMA2), evoked robust inflammatory/immunological response in mouse and human macrophages, by inducing the secretion of the inflammatory cytokine interleukin-1 $\beta$  (IL-1 $\beta$ ) (Sunasee et al., 2015). In this study, we advanced a step further in the understanding of the mechanisms of the immunological responses evoked by a cationic CNCs (CNCs-poly(N-3-aminopropylmethacrylamide), CNCs-poly(APMA)), and an anionic CNCs (CNCs-poly(N-isopropylacrylamide), CNCs-poly(NIPAAm)) by analyzing mitochondria-derived ROS and mitochondrial function as well as changes in lysosomal acidification and ER stress.

#### 2. Methods

#### 2.1. Materials

Freeze-dried sulfated CNCs in their neutralized sodium salt forms were obtained from Innotech. Octyl phenoxy polyethoxyethanol (Triton-X100), sodium dodecyl sulfate (SDS), β-mercaptoethanol (β-ME), acridine orange and 4',6-diamidino-2-phenylindole (DAPI) were purchased from Sigma Aldrich. Mitochondrial superoxide indicator (MitoSOX™ Red) were obtained from Molecular Probes® (Invitrogen™). ER-Tracker™ Green (BODIPY™ FL Glibenclamide) and Lysosensor Green DND-189 were obtained from Thermo Fisher, and 5,5',6,6'-tetrachloro-1,1',3,3'-tetraethylbenzimi-dazolcarbocyanine iodide (JC-1) from Cayman. Caspase-Glo® 1 assay kit and ATP bioluminescence kit were obtained from Promega and Biovision, respectively. Lipopolysaccharide (LPS, E. coli 0111:B4) and phorbol myristate acetate (PMA) were purchased from InvivoGen. NLRP3 and IL-1 $\beta$  antibodies were bought from Adipogen and Biovision, respectively. Catalase was purchased from EMD and oxidized peroxiredoxin (PrxSO<sub>3</sub>,) from AbFrontier. Caspase 1, peroxiredoxin 1 (Prx1), thioredoxin 2 (Trx2) antibodies were obtained from Abcam, as well as IgG horseradish peroxidase-linked secondary mouse and rabbit antibodies. Superoxide dismutase 1 antibody (SOD1)

was purchased from Proteintech and superoxide dismutase 2 (SOD2) and  $\beta\mbox{-}actin$  antibodies were obtained from Thermo Fisher. Autophagy-related protein LC3 B (LC3B) and autophagy-related protein 13 (ATG13) antibodies obtained from Cell Signaling, and protein disulfide isomerase antibody (PDI) from ENZO. Enhanced chemiluminescence substrate (ECL) was purchased from Pierce. Mouse and human TNF  $\alpha$  and human IL-1 $\beta$  ELISA sets were purchased from BD Biosciences and mouse IL-1 $\beta\slash$ /IL-1F2 DuoSet ELISA and TMB ELISA substrate from R&D Systems. All reagents were of analytical grade.

#### 2.2. Preparation of cationic and anionic surface functionalized CNCs

CNCs-poly(*N*-3-aminopropylmethacrylamide) Cationic CNCs. (CNCs-poly(APMA)) and anionic CNCs, CNCs-poly(N-isopropylacrylamide) (CNCs-poly(NIPAAm)) were synthesized recently in our laboratory using surface-initiated single-electron transfer living radical polymerization method (Sunasee et al., 2016; Jimenez et al., 2017). The resulting materials were extensively purified using repeated centrifugations and dialysis over a week. The cationic and anionic nature of the surface modified CNCs were confirmed by zeta potential measurements at neutral pH which indicated values of +45.2 mV and - 22.4 mV for CNCs-poly(APMA) and CNCs-poly(NIPAAm) respectively. Their chemical structures, FTIR and DLS data are provided in the supplemental section. Detailed syntheses and characterization are fully described elsewhere (Jimenez et al., 2017; Hemraz et al., 2014)

#### 2.3. Cell Culture and experimental conditions

Mouse macrophage-like cell line (J774A.1) and human monocyic cell line (THP-1) were seeded at  $1 \times 10^6$  cells/mL in RPMI 1640 supplemented with 10% fetal bovine serum (FBS), penicillin, streptomycin and L-glutamine, and incubated at 37 °C in a 5% CO<sub>2</sub>-supplemented atmosphere for at least 24 h before the appropriate treatments. THP-1 cells were stimulated with PMA 20 ng/mL, for 48 h prior to any treatment. The peripheral blood mononuclear cells (PBMCs) were extracted from Leukotrap blood filters from healthy blood donors obtained from UVM Health Network-CVPH North Country Regional Blood Center, Plattsburgh, NY. To recover blood cells, the filter was reverse flushed with 3 × 50 mL of calcium and magnesium-free PBS and PBMCs were isolated using a separation medium (LSM) followed by centrifugation. The PBMCs were seeded at  $1 \times 10^6$  cells/mL in RPMI 1640 medium as described above and incubated at 37 °C in a 5% CO2-supplemented atmosphere for overnight before the appropriate treatments. J7744A.1, PBMCs or PMA- stimulated THP1 the cells were primed with 100 ng/mL of LPS and 4h later, 50 µg/mL of CNCs-poly(APMA) or CNCs-poly (NIPAAm) were concomitantly added for a total of 24 h of total treatment. In this study, we used 50 µg/mL CNCs-poly(APMA) and CNCspoly(NIPAAm) to perform all experiments, since we have previously demonstrated that at this concentration, these nanomaterials have no or minimal effect on mammalian cell viability (Jimenez et al., 2017). In another study involving cationic CNCs derivatives, 50 µg/mL was the effective dose used to evoke the desired inflammatory response in J774A.1 cell line as well as in PBMCs (Sunasee et al., 2015).

#### 2.4. Detection of IL-1 $\beta$ and TNF- $\alpha$ in cell supernatants

Secreted cytokines into the cell supernatants were quantified by enzyme-linked immunoabsorbent assay (ELISA), according to the manufacturer's instruction.

#### 2.5. SDS-PAGE and immunoblotting

Cell lysates were prepared using lysis buffer (50 mM Tris, pH 7.4, 150 mM NaCl, 2 mM EDTA 0.2% Triton™ X-100, 0.3% IGEPAL® and protease inhibitor cocktail). Equal amounts of cell lysates were

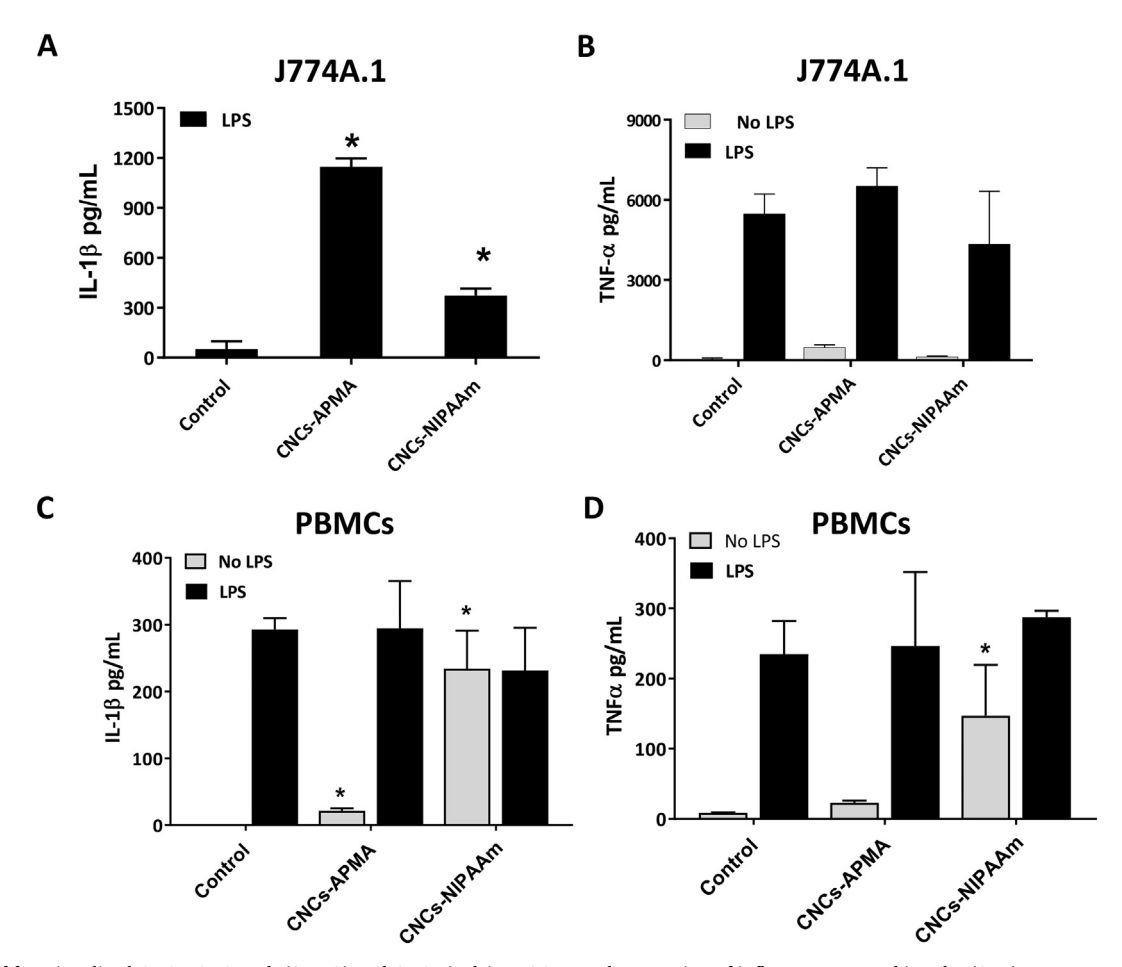


**Fig. 1.** Effect of functionalized CNCs, CNCs-poly(APMA) and CNCs-(poly)NIPAAm on the secretion of inflammatory cytokines by (A, B) Mouse macrophage-like cell line (J774A.1) or (C,D) peripheral blood mononuclear cell (PBMCs). Secreted IL-1β (A, C) or TNFα (B,D) were quantified in the cell supernatants by ELISA. Data were means  $\pm$  S.D. from triplicate experiments. \*p < .1 compared to the respective control. For simplicity we abbreviated the compounds as follow, CNCs-poly (NIPAAm) = CNCs-NIPAAm and CNCs-poly(APMA) = CNCs-APMA.

subjected to SDS-PAGE (12% sodium dodecyl sulfate polyacrylamide gel). The polyvinylidene difluoride (PVDF) membrane was blocked for 1 h with 5% milk in PBS containing 0.05% Tween®20 (PBST) and incubated with primary antibodies overnight at 4 °C, followed by 1 h incubation with secondary antibodies. The membranes were developed using enhanced chemiluminescence substrate (ECL) according manufacturer's instructions and images captured using ChemiDoc $^{\text{TM}}$  MP Imaging System coupled with Image Lab $^{\text{TM}}$  software.

#### 2.6. In situ detection of IL-1β, NLRP3

Detection of IL-1 $\beta$ , NLRP3 was performed in fixed cells with paraformaldehyde 4% followed by permeabilization with triton 0.2% for 10 min and blocking with 1% BSA for 1 h. Cells were incubated overnight at 4 °C with respective primary antibodies and subsequently with Alexa Fluor-conjugated secondary antibodies for 1 h at room temperature. Nuclei were counterstained with DAPI. Immunofluorescence was visualized with an Olympus BX53 fluorescence microscope coupled with Olympus DP73 digital camera and analyzed using ImageJ software.

#### 2.7. Detection of mitochondria-derived ROS

Cells were loaded with 2.5 µM MitoSOX™ Red, a cell-permeable cationic dihyrdoethidium dye that is targeted to the mitochondria and detects ROS, producing bright red fluorescence. After 10 min at 37 °C, cells were rinsed with PBS and nuclei were counterstained with DAPI.

Cell images were captured with BioRad ZOE<sup>TM</sup> Cell Imager and respective pictures were analyzed using ImageJ software. Antimycin A  $40\,\mu\text{g/mL}$  was utilized as positive control (Supplemental material).

#### 2.8. Detection of mitochondrial membrane potential ( $\Delta \psi m$ )

After treatments, cells were incubated in fresh medium containing  $5\,\mu\text{g/mL}$  of 5,5′,6,6′-tetrachloro-1,1′,3,3′-tetraethylbenzimidazol-carbocyanine iodide (JC-1) for 15 min, followed by prompt capture of the images using BioRad ZOE<sup>TM</sup> Cell Imager. Images were analyzed using ImageJ software. Green fluorescence indicates monomer at depolarized (unhealthy mitochondria) and red indicates J-aggregate at hyperpolarized (healthy mitochondria) membrane potentials.

#### 2.9. In situ analysis of endoplasmic reticulum (ER) and acidic organelles

ER-Tracker<sup>TM</sup> Green (green-fluorescent BODIPY® FL) is cell-permeant, live-cell stain that is highly selective for the endoplasmic reticulum (ER). Acridine orange (AO) is a hydrophobic green fluorescent molecule that, within acidic vesicles, becomes protonated and trapped within the organelle forming aggregates that emitted bright red fluorescence (Thome et al., 2016). LysoSensor<sup>TM</sup> Green DND-189 is almost non-fluorescent at neutral pH, and when inside acidic compartments, it becomes green fluorescent. After treatments, cells were incubated with 1  $\mu$ M of ER-Tracker<sup>TM</sup> Green or LysoSensor<sup>TM</sup> Green DND-189 for 15 and 45 min, respectively. Alternatively, cells were incubated with AO 4  $\mu$ g/mL for 10 min. After incubations with the respective fluorescent probes,

the images were captured in a BioRad  $ZOE^{TM}$  Cell Imager or Olympus BX53 fluorescence microscope coupled with Olympus DP73 digital camera and analyzed using ImageJ software.

#### 2.10. Measurement of ATP content

Assessment of ATP content was performed using the ATP bioluminescence assay kit following the manufacturer's instructions. After treatments, intracellular ATP was assessed in cell lysates (Triton  $^{\text{\tiny M}}$  X-100 1%, PBS) and 10  $\mu\text{L}$  of the lysates were added to 90  $\mu\text{L}$  of ATP reaction buffer. Alternatively, 10  $\mu\text{L}$  of cell culture medium was added to 90  $\mu\text{L}$  of reaction buffer to detect extracellular ATP. The luminescence was measured using a Synergy H1 Hybrid Multi-Mode Microplate Reader (BioTek). Values were expressed as relative fluorescence units (RLU).

#### 2.11. Statistical analysis

The data was statistically analyzed by using the one-way analysis of variance test, followed by Turkey's multiple comparison test, using GraphPad Prizm 7.01 software. Statistical significance was defined as p < .1 or 0.05.

#### 3. Results

## 3.1. Cationic CNCs-poly(APMA) induced stronger immune response in LPS-stimulated cells than anionic CNCs-poly(NIPAAm)

In this study, we first investigated whether an anionic CNCs derivative, CNCs-poly (NIPAAm) would cause similar immunological response to the cationic CNCs-poly(APMA). The detailed synthesis and characterization of these nanomaterials were described elsewhere (Jimenez et al., 2017; Hemraz et al., 2014). The data presented in Fig. 1A indicates that the cationic CNCs-poly(APMA) induces greater IL-1β secretion in LPS-primed mouse macrophage-like cells (J774A.1), but no effect in non-primed cells. TNFa secretion, a NLRP3 inflammasome-independent cytokine (Wilson et al., 2014), was not further increased in the presence of functionalized CNCs in LPS-primed cells (Fig. 1B black bars). A noticeable increase in presence of CNCs-poly (APMA) was observed in non-primed cells (Fig. 1B, gray bars). CNCspoly(NIPAAm) led to a greater secretion of both cytokines, IL-1β and TNF-α in non-primed PBMCs (Fig. 1C and D gray bars). Since LPS alone is able to induce both TNF- $\alpha$  and IL-1 $\beta$  secretion (Catalan et al., 2015) in PBMCs, no further changes in the levels of these cytokines were observed upon treatment with functionalized CNCs (Fig. 1D and C black bars). CNCs-poly(APMA) was the only CNCs that caused increases in the IL-1 $\beta$  secretion in differentiated and primed-human monocytic cell line (THP1) (Fig. 1- supplemental material). The secretion of IL-1 $\beta$  depends on the synthesis of NLRP3 inflammasome precursors. The analysis of the levels of intracellular inflammasome components confirmed that the proteins NLRP3 and pro-IL-1ß were mildly and dramatically increased in presence of LPS, respectively (Fig. 2A). An additional modest increase in pro-IL-1 $\beta$  in primed cells (Fig. 2A, second panel), and a decrease in pro-caspase-1 in non-primed cells in the presence of CNCspoly(APMA) was also observed (Fig. 2A, third panel). Interestingly, in both primed and non-primed cells treated with CNCs-poly(APMA), a small decrease in NLRP3 intracellular level was detected (Fig. 2A, top panel). Changes in intracellular localization of the NLRP3 inflammasome components can also affect the outcome of secreted cytokines (Guglielmo et al., 2017). Overall, the image analysis showed that both NLRP3 (red fluorescence) and pro-IL-1β (green fluorescence, referred as IL-1β) were enhanced in cells treated with LPS only (Fig. 2B). Surprisingly, with functionalized CNCs, the pattern of distribution and fluorescence intensity changes substantially. Treatment with CNCs-poly (APMA) alone increased fluorescence intensity for both IL-1ß and NLRP3 (Fig. 2B, graph below the figure) and appeared to induce

accumulation of IL-1ß in "vesicle-like" structures as indicated by punctuated bright green fluorescence (Fig. 2B, white arrows). In primed cells, however, the presence of CNCs-poly(APMA) caused a general decrease in NLRP3 and IL-1 $\beta$ , which is consistent with higher IL-1 $\beta$ secretion in this experimental condition. CNCs-poly(NIPAAm), also led to a decrease in NLRP3 staining in non-primed cells. Furthermore, in primed cells the same nanomaterial caused an increase in NLRP3 staining and no changes in IL-1 $\beta$  in both primed and non-primed cells. (Fig. 2B, bottom panels and graph). Caspase-1, a cysteine-aspartate specific protease, is a member of caspase family and it is responsible for processing pro-IL-1\beta in its mature and active form (Afonina et al., 2015). Next, we investigated the intracellular and extracellular activity of caspase-1. Surprisingly, in differentiated THP-1 cells, CNCs-poly (APMA) diminished the intracellular caspase-1 activity in the presence and absence of LPS (Fig. 2A supplemental) and the extracellular activity of caspase-1 was not significantly affected in any tested conditions (Fig. 2B supplemental). In mouse macrophage-like cell line (J774A.1), a similar trend was observed in which CNCs-poly(APMA) decreased intracellular caspase-1 activity, although it was not statistically significant (Fig. 2C supplemental). These collective results indicate that the cationic CNCs, CNCs-poly(APMA) has a greater impact in the IL-1β secretion by LPS-stimulated myeloid cells than the anionic CNCs, CNCspoly(NIPAAm), and it appears that the mechanisms by which these nanomaterials exert their immunomodulation vary.

## 3.2. Anionic and cationic CNCs impact mitochondrial function in different manner

Usually, the activation of NLRP3 inflammasome and IL-β secretion are associated with increases in mitochondrial ROS (Sunasee et al., 2015; Jabaut et al., 2013). Despite greater effect on the secretion of IL-1β. CNCs-poly(APMA) caused minor increases in mitochondria-derived ROS in non-stimulated cells and surprisingly showed a robust decrease in the presence of LPS. Conversely, CNCs-poly(NIPAAm) showed robust increases in mitochondria-derived ROS in the absence of LPS, and no changes in the presence of LPS (Fig. 3A). Increases in mitochondriaderived ROS can impact mitochondrial function and ultimately may also affect mitochondria membrane potential ( $\Delta\Psi$ m) and levels of ATP (Brookes et al., 2004). Changes in mitochondrial membrane potential  $(\Delta\Psi)$  can be used as biomarker of mitochondrial function. JC-1 dye occurs as a green-fluorescent (monomer) indicating depolarized membrane potentials, and as a red-fluorescent (J-aggregate) indicating hyperpolarized membrane potentials. When the ratio between red and green is analyzed, our results indicate that both functionalized CNCs alone increased polarization of the membrane since the ratio is slightly greater than control cells (Fig. 3B, graph, gray bars). However, in LPSstimulated cells CNCs-poly(APMA) demonstrated a decrease in polarization while CNCs-poly(NIPAAm) indicated an increase. (Fig. 3B, graph, black bars). We next investigated whether changes in  $\Delta\Psi m$ would affect ATP levels. Our results indicated that in primed-cells, CNCs-poly(APMA) significantly decreased the intracellular levels of ATP (Fig. 4A, black bars) and no significant changes in extracellular ATP (Fig. 4B, black and gray bars). The decrease in intracellular ATP content caused by CNCs-poly(APMA) in LPS-stimulated cells might be associated with the lowering in mitochondrial membrane potential observed with the same experimental condition. The electrical potential  $(\Delta \psi)$  is a requirement for torque generation in the motor of the ATP synthase and therefore also needed to produce ATP (Dimroth et al., 2000). Overall, our data suggest that cationic CNCs-poly(APMA) has a stronger impact on the mitochondrial function in LPS-stimulated cells, while the anionic CNCs-poly(NIPAAm) displays a greater impact on mitochondria-derived ROS, especially in non-stimulated cells.

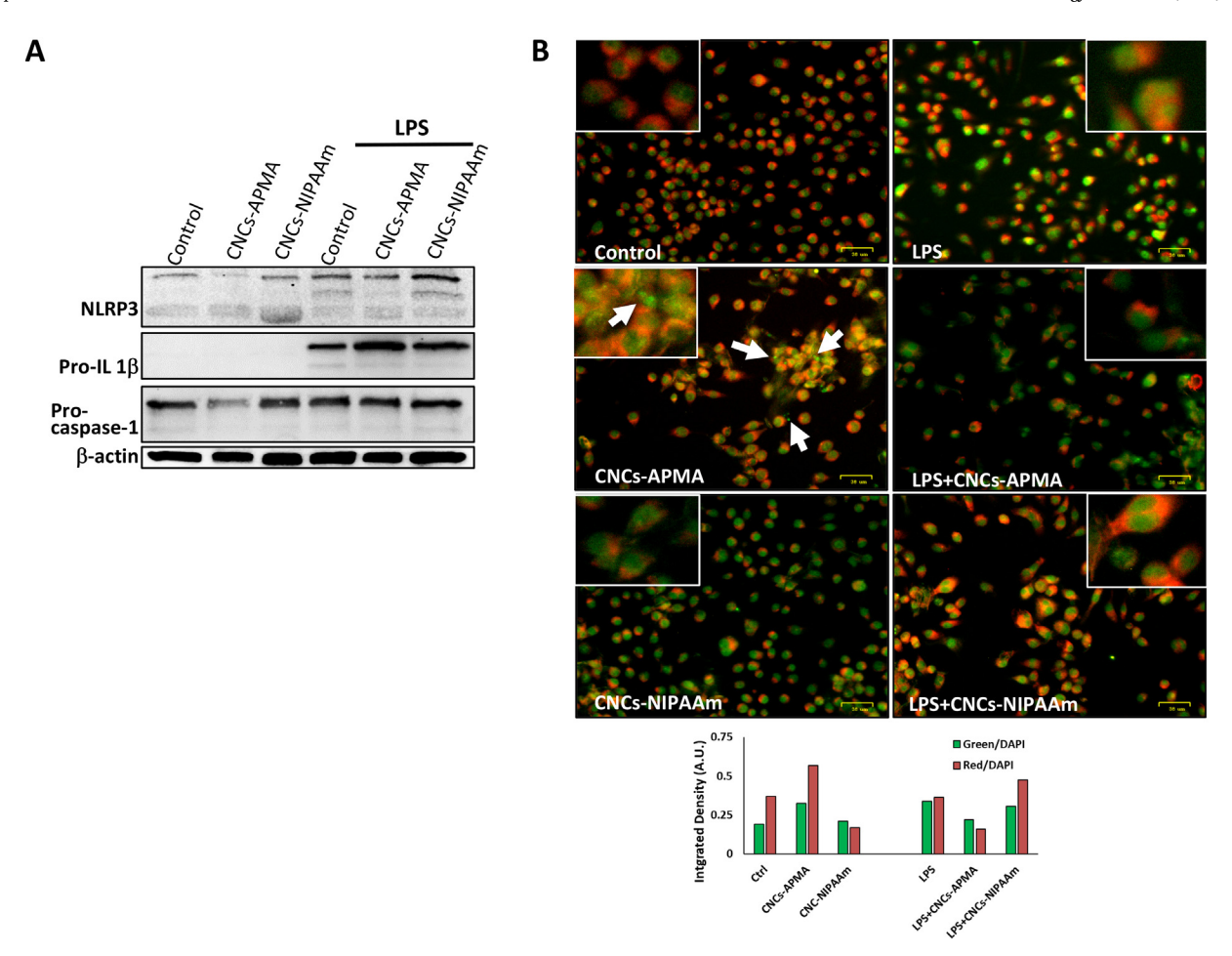


Fig. 2. Effect of functionalized CNCs on the level and distribution of intracellular NLRP3 inflammasome components in J774A.1 cells. (A) Intracellular inflammasome components NLRP3, pro-IL-1 $\beta$ , pro-caspase-1 were analyzed by Western blotting in the cell lysates.  $\beta$ -actin was used as loading control. (B) Alternatively, expression and intracellular distribution of IL-1 $\beta$  (green) and NLRP3 (red) was detected using immunofluorescence. DAPI (blue) was used as nuclei staining. The pixel intensity was analyzed using ImageJ and expressed as integrated intensity corrected by nuclear staining (DAPI) (graph at the bottom of images). The bar at the bottom of each panel is equivalent to 38  $\mu$ m. The white arrows highlight the punctuated green fluorescence. (For interpretation of the references to colour in this figure legend, the reader is referred to the web version of this article.)

# 3.3. Anionic and cationic CNCs cause changes in the intracellular level of antioxidant enzymes

Considering that the activation of NLRP3 inflammasome/IL-1 B axis by nanomaterials is associated with increases in ROS, including mitochondrial ROS (Sunasee et al., 2015), we next investigated the antioxidant response by analyzing the intracellular levels of antioxidant enzymes. Again, we observed opposite impact of these functionalized CNCs on various antioxidant enzymes, especially in non-stimulated cells. In general, CNCs-poly(APMA) appeared to lower the levels of catalase, SOD1, Prx1 and oxidized peroxiredoxins PrxSO3, while CNCspoly(NIPAAm) had the opposite effect, when compared with unstimulated cells (Fig. 5). In addition, CNCs-poly(APMA) decreased, and CNCs-poly(NIPAAm) increased the intracellular level of catalase, Prx1 and PrxSO<sub>3</sub> in LPS-stimulated cells, SOD1, however, appeared to be similarly affected only in non-primed cells treated with CNCs-poly (APMA) or CNCs-poly(NIPAAm) (Fig. 5). Interestingly, for the mitochondrial antioxidant enzymes, SOD2 and Trx2 (Li et al., 2013), both nanomaterials increased the intracellular levels of these enzymes in non-stimulated and stimulated cells, at different degree. CNCs-poly (NIPAAm) caused the greatest increase on these mitochondrial enzymes (Fig. 5, 3<sup>rd</sup> and 4<sup>th</sup> panels), which is consistent with the augmented production of mitochondria-derived ROS, at least in non-stimulated cells (Fig. 3A, graph gray bars).

## 3.4. CNCs-poly(NIPAAm) caused greater lysosome acidification and ER stress response than CNCs-poly (APMA)

The internalization of nanoparticles (NPs) allows them to reach the subcellular locations and cause disturbance in diverse organelles such as mitochondria, endoplasmic reticulum (ER), among others (Zhang et al., 2016). The dysfunctional organelles and/or macromolecules can trigger autophagy. Autophagy is a complex cellular process that involves the fusion of autophagosome with lysosome, among other events. When autophagy is induced or lysosomes are impaired, LC3 protein will be cleaved into LC3-I and then lipidated leading to the accumulation of LC3-II (Mizushima et al., 2010). Therefore, the increase of LC3-II protein levels can be an indicative of autophagy and or lysosomal impairment. First, we analyzed the impact of the functionalized CNCs on the lysosomes acidification using a green fluorescent probe. Our results indicated that all the treatments caused an overall decrease in lysosomal pH, as the green fluorescence became more intense, in comparison to the control untreated cells (Fig. 6A). Specifically, the treatment of LPS-stimulated cells with CNCs-poly(NIPAAm) appeared to induce the greatest lysosomal acidification (Fig. 6A, graph black bars). As expected, chloroquine, a well-known lysosomotropic agent that prevents lysosomal acidification (Steinman et al., 1983), showed the lowest green florescence (Fig. 6A, bottom panel). In a secondary approach, we also detected the formation of acidic vesicular organelles (AVOs) using acridine orange staining. We observed that the

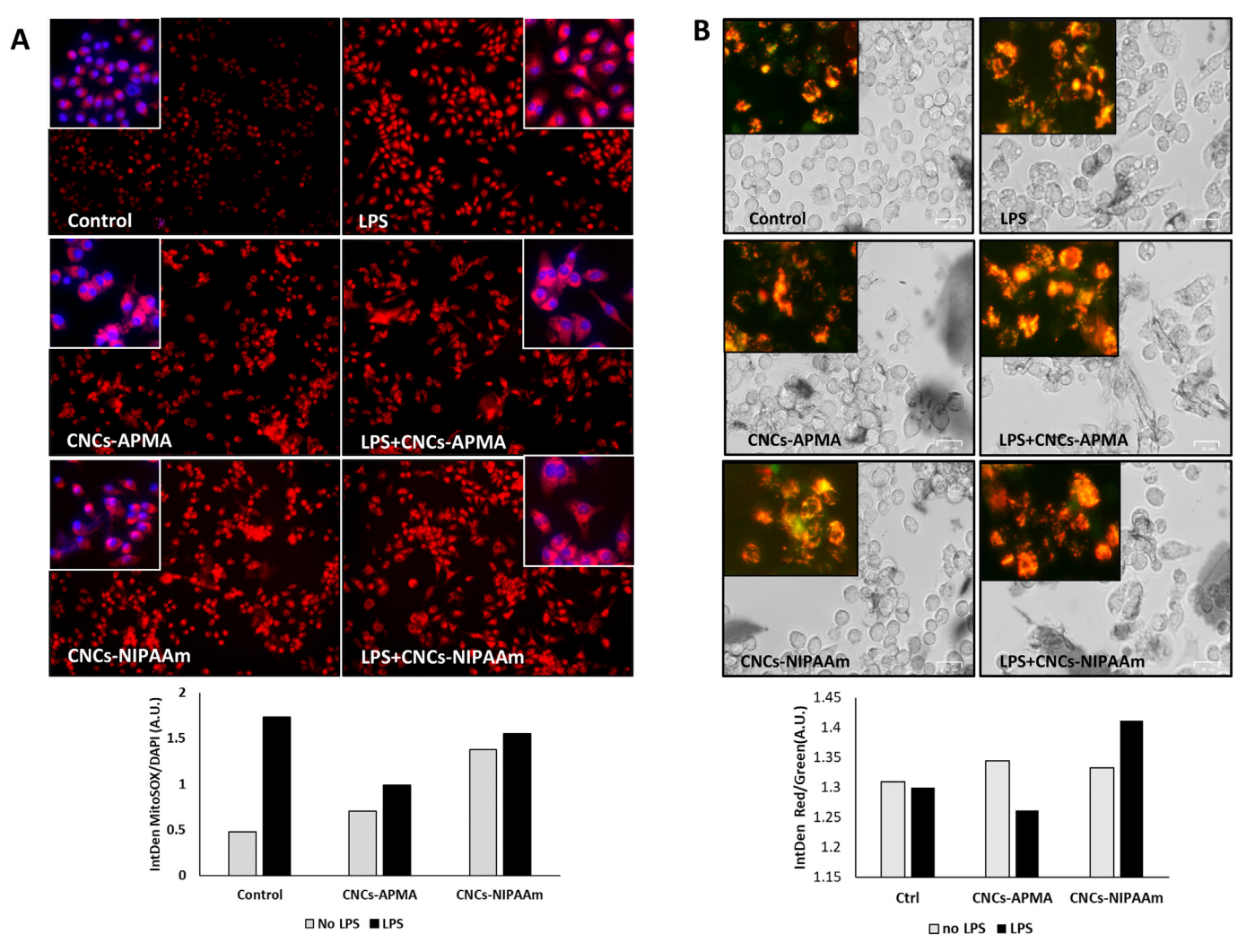


Fig. 3. Effect of functionalized CNCs on the formation of mitochondria-derived ROS and on the membrane potential ( $\Delta\psi m$ ) in J774A.1 cells. (A) Mitochondrial ROS were promptly analyzed utilizing a fluorescence cell imager at  $200 \times magnification$ . The insert on the top left of each panel represents a merged zoomed image of DAPI and MitoSOX. The pixel intensity was analyzed using ImageJ and expressed as integrated intensity (graph on the bottom of the figure). (B) JC-1 dye was added to the live cells and mitochondrial membrane potential ( $\Delta\psi m$ ) was promptly analyzed in a fluorescence cell imager. Green fluorescence indicates depolarized (monomer form of JC-1, unhealthy mitochondria) and red indicates hyperpolarized (J aggregate, healthy mitochondria). The red/green ratio was calculated using integrated intensity of red and green channels measured by ImageJ software (graph at the bottom of the figure). The bar at the bottom of each panel is equivalent to 25  $\mu m$ . (For interpretation of the references to colour in this figure legend, the reader is referred to the web version of this article.)

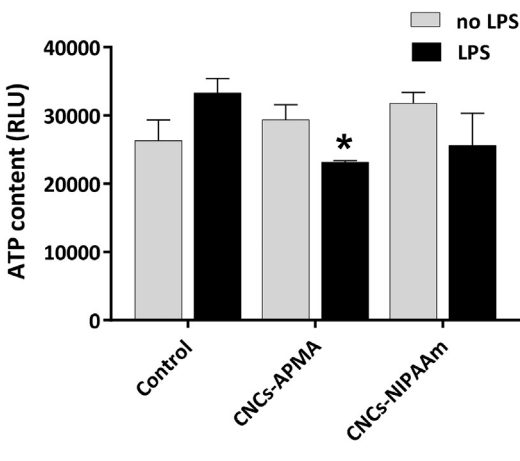
CNCs-poly(NIPAAm) not only induced the greatest red/green ratio (Fig. 6B, graph), but also induced the greatest AVOs formation indicated by punctuated red staining on the cells, in LPS-stimulated cells (Fig. 6B, bottom panels, white arrows). The ER has a key role in the synthesis, folding, and structural maturation of proteins produced in the cell. We investigated the overall distribution of ER using green fluorescence probe followed by cell image analysis. Our results demonstrated that there are no major differences in ER distribution, in any condition tested (Fig. 3, supplemental material). When misfolded proteins accumulate above a critical threshold as consequence of stressful conditions, a rapid and coordinated biochemical response involving ER stress response is triggered (Tesei et al., 2018; Oslowski and Urano, 2011). The unfolded protein response (UPR) is one of the major ER stress responses, which can lead to autophagy (Hoyer-Hansen and Jaattela, 2007). Among the proteins that participated in the UPR, there is PDI, which is responsible for the proper folding of proteins (Oslowski and Urano, 2011). Atg13 and LC3 I-II are proteins associated with induction and elongation/closure of autophagosome, respectively (Lebovitz et al., 2012). Our results showed that in non-stimulated cells, CNCs-poly(NIPAAm) induced a slight increase in both ATg13 and PDI

proteins and CNCs-poly(APMA) had an opposite effect (Figure -7 top and bottom panels). In LPS-stimulated cells, both CNCs-poly(APMA) and CNCs-poly(NIPAAm) decreased PDI levels and increased Atg13, and CNCs-poly(NIPAAm) showed a more prominent effect. Although J774A.1 cells showed practically undetectable basal level of LC3-I (top band), we did not notice any robust changes in the levels of this autophagy marker in any conditions tested (Fig. 7). In general, these data suggest that CNCs-poly(NIPAAm) has a greater impact on lysosomal acidification and on the ER stress response than CNCs-poly(APMA).

#### 4. Discussion

The interest in utilizing derivatives of CNCs for multiple biomedical application has been increasing in the recent years. CNCs are versatile platforms that show variation in size and dispersion depending on the methods of extraction and preparations, which can impact their cytotoxicity (Endes et al., 2015). Regardless of the methods of preparation and extraction of pristine CNCs, these cellulose-based nanomaterials are suitable for surface functionalization with an array of polymers, which generate an even more chemically diverse group of related

## A - Intracellular



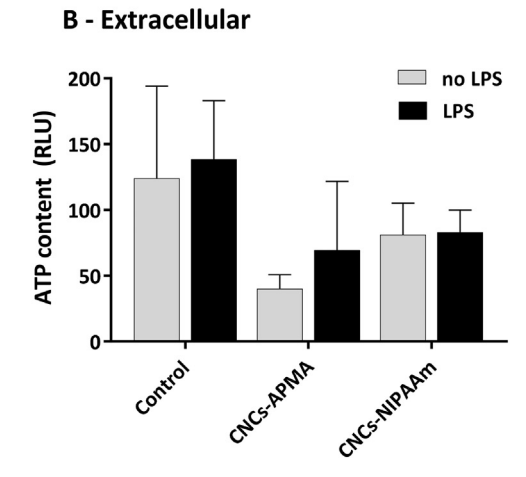


Fig. 4. Effect of functionalized CNCs on the intracellular and extracellular ATP content in J774A.1 cells. (A) Cell lysates (intracellular ATP) and (B) supernatants (extracellular ATP) analyzed with ATP bioluminescence assay kit. Data are expressed as relative luminescence units (RLU). Data were means  $\pm$  S.D. from triplicate experiments. \*p < .05 compared to control.

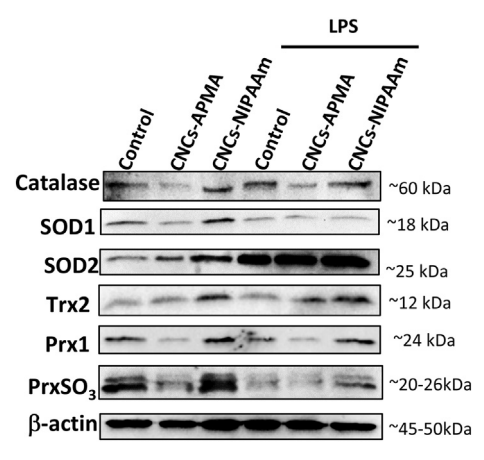


Fig. 5. Effect of functionalized CNCs on the level antioxidant enzymes in J774A.1 cells. The level of the antioxidant enzymes catalase, superoxide dismutase 1 and 2 (SOD1 and SOD2), thioredoxin 2 (Trx2), peroxiredoxin 1 (Prx1) and oxidized peroxiredoxins (PrxSO $_3$ ) were analyzed by Western blotting in the cell lysates. β-actin was used as loading control.

nanomaterials. Nevertheless, this physico-chemical diversity can lead to a diverse biological response (Sunasee et al., 2016). Analysis of cytotoxicity is the primary biological response used as a standard assay, but other biological responses are equally important especially when these nanomaterials are designed for biomedical applications. Previously, we described the synthesis, characterization and cytotoxicity of the CNCspoly(NIPAAm) and CNCs-poly(APMA) with zeta potentials and hydrodynamic diameter values of  $-22.4 \pm 1.4 \,\mathrm{mV}$  and  $+45.2 \pm 1.3 \,\mathrm{mV}$ ,  $126.9 \pm 0.4 \,\mathrm{nm}$  and  $154.6 \pm 3.6 \,\mathrm{nm}$  respectively. Despite their physico-chemical differences, these nanomaterials showed minimal cytotoxicity (Jimenez et al., 2017). In this study, we compared the in-vitro immunological response induced by a cationic and an anionic surface functionalized CNCs and explored the potential mechanisms by which these nanomaterials evoked such response. We observed that both nanomaterials showed an immunological response in cell-based assays, however the intensity and the potential mechanisms by which they evoke this response appeared to be different. The more pronounced effect observed with CNCs-poly(APMA) on stimulated murine macrophages can be explained, at least in part, by the greater intracellular induction of the pro-IL-1ß as indicated by western blotting and confirmed by disappearance of the IL-1\beta displayed by cell imaging. The canonical mechanism of NLRP3 inflammasome activation involves two

simultaneous and independent steps: synthesis of precursors in a nuclear factor kappa B (NF- $\kappa$ B)-dependent manner, and oligomerization of the NLRP3 complex, followed by secretion of IL- $\beta$  (Pellegrini et al., 2017). We and others have demonstrated that cationic functionalized nanoparticles can indeed induce pro-IL-1 $\beta$  synthesis and secretion of its active form, IL- $\beta$  (Lunov et al., 2011; Sunasee et al., 2015). On non-stimulated human cells, however, CNCs-poly(APMA) alone might have induced a potential synergetic effect, since it showed greater increases in both IL-1 $\beta$  and TNF $\alpha$  secretion. In fact, it is known for a long time that TNF $\alpha$  induces IL- $\beta$  production in animal model (Dinarello et al., 1986).

These nanomaterials also have different effects on the mitochondria-derived ROS and mitochondrial function. CNCs-poly(NIPAAm) demonstrated to induce greater amounts of mitochondria-derived ROS, especially in non-stimulated murine macrophages and less changes in mitochondrial function, while CNCs-poly(APMA) had opposite effect. CNCs-poly(NIPAAm) induced a greater enzymatic antioxidant response than CNCs-poly(APMA), mainly in the mitochondrial Trx2 (Arner, 2009) and SOD2 (Candas and Li, 2014) also in non-stimulated murine macrophages. It is known that in order to overcome increases in ROS and prevent an oxidative stress the antioxidant enzymes are upregulated (Birben et al., 2012). CNCs-poly(APMA) appears to have a greater impact on the ATP synthesis as indicated by decreases in intracellular ATP in stimulated murine macrophages which correlates with a less polarized membrane. The correlation between ATP synthesis and mitochondrial membrane potential is not surprising because it is well known that the ATP synthesis is dependent on the membrane potential of mitochondria (Liberman et al., 1961). In fact, positively charged particles tend to induce mitochondrial dysfunction including hyperpolarization or depolarization of mitochondria membrane and autophagy (Malugin and Ghandehari, 2011), which could lead to impairment of ATP synthesis. Interestingly, the reduction in intracellular ATP can lead to NLRP3 inflammasome activation caused by crystal stimulation, such as monosodium urate (MSU)(Nomura et al., 2015). Several biomarkers have been identified in different phases of the complex process of autophagy, including ATg13 and LC3, which are used to monitor autophagy induction. We did not observe a significant impact of either nanoparticle on the induction of autophagy as indicated by no changes in LC3I-II western blotting.

The impact on lysosome acidification and ER stress also highlights the differences between these nanomaterials. Both nanomaterials caused increases in acidic vesicles and lysosomal acidification and in stimulated and non-stimulated cells, however CNCs-poly(NIPAAm)

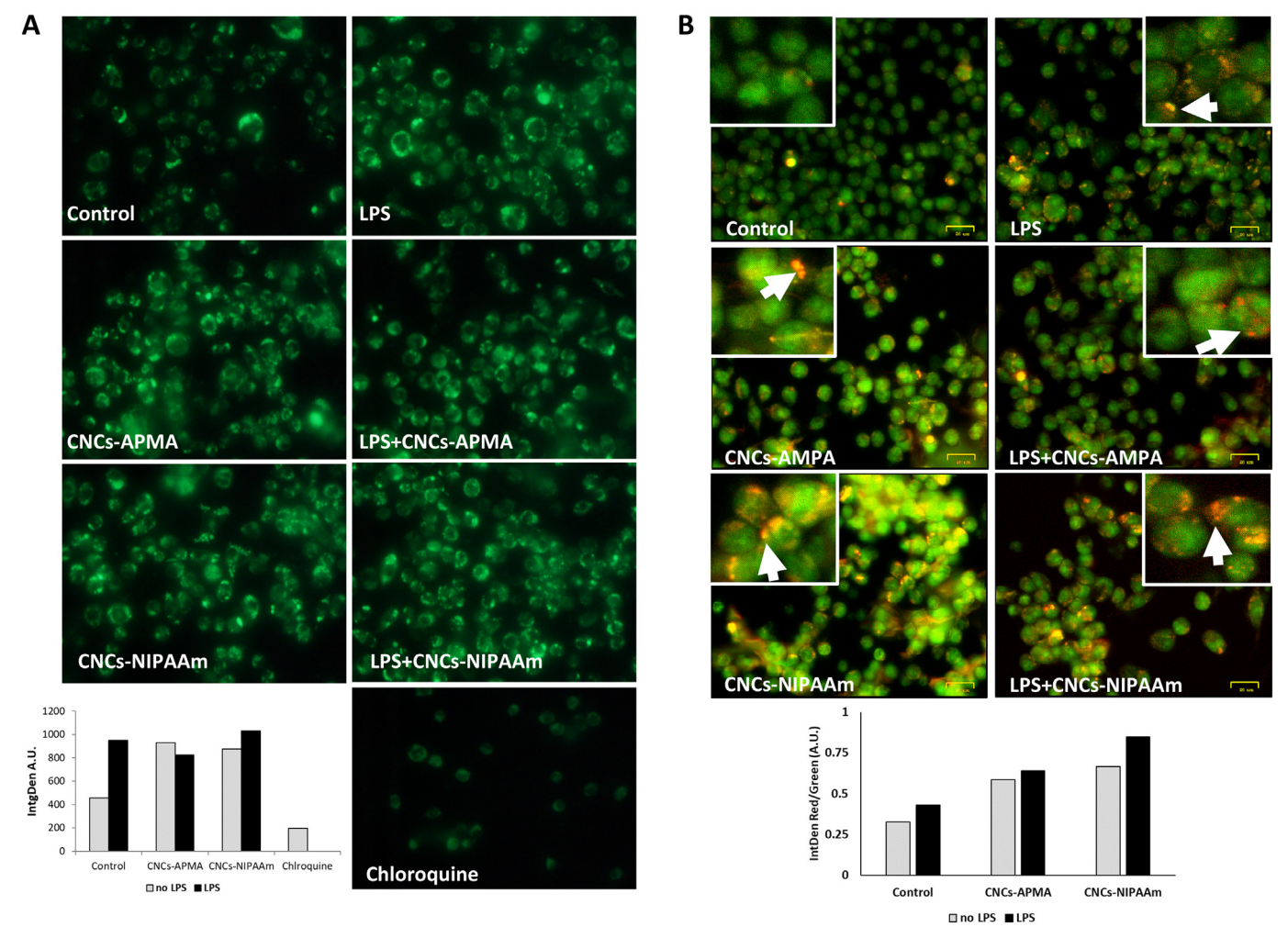


Fig. 6. Effect of functionalized CNCs on the organelle acidification in J774A.1 cells. (A) LysoSensor green analyzed utilizing a fluorescence microscope at  $400 \times \text{magnification}$ . Chloroquine ( $100 \, \mu\text{M}$ , 5 h negative control) was used as lysosomotropic reagent to inhibit lysosome acidification. (B) Alternatively, acridine orange was used to detect acidic vesicular organelles (AVOs) and images were immediately capture using a cell imager. The bar at the bottom of each panel is equivalent to  $26 \, \mu\text{m}$ . The white arrows highlight the punctuated orange fluorescence, indicating the presence of AVOs. The pixel intensity was analyzed using ImageJ and expressed as integrated intensity (graph on the bottom of both figures). (For interpretation of the references to colour in this figure legend, the reader is referred to the web version of this article.)

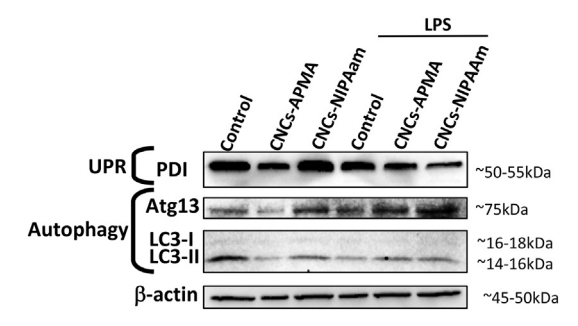


Fig. 7. Effect of functionalized CNCs on the level of proteins involved in unfolded protein response (UPR) and autophagy in J774A.1 cells. The UPR marker, protein disulfide isomerase (PDI) as well as autophagy markers, autophagy related protein 13 (Atg13) and microtubule-associated protein 1A/1B-light chain 3 (LC-3) were analyzed by Western blotting in the cell lysates.  $\beta$ -actin was used as loading control.

caused the greatest effect in both conditions. Healthy lysosomes are acidic (pH 4.5–5.0), and small fluctuations towards the acidic environment (Mindell, 2012) is expected during the phagocytosis process. The fusion of lysosomes and phagosomes generates the phagolysosomes (Aderem and Underhill, 1999) wich is considered an acidic vesicular

organelles (AVOs). It is not a surprise that charged CNCs derivatives caused lysosomal acidification, since a more likely process of entry of these nanomaterials would be via phagocytosis (Dobrovolskaia, 2015). Although our previous study suggested that size and charge may not be directly related with cytotoxicity, we observed that indeed CNCs-poly (NIPAAm) appears to cause cell enlargement and elongation (Jimenez et al., 2017). This previous observation on the apparent changes in cell morphology can be associated with the greater effects of CNCs-poly (NIPAAm) on the formation of acidic vesicular organelles (AVOs), suggesting a greater phagocytic activity by the macrophages. Although it has been reported long time ago that positively charged particles are more prone to phagocytosis by macrophages (Matsui et al., 1983), we do not exclude the possibility that CNCs-poly(NIPAAm) induced stronger phagocytic activity because of potential interactions of this anionic nanomaterial with serum proteins. The process by which particles in general become covered with opsonin proteins is called opsonization (Owens and Peppas, 2006; Gustafson et al., 2015). Both opsonin protein composition and conformation on the particle surface influence how nanoparticles interact with macrophage surface receptors and mediate phagocytic recognition (Gustafson et al., 2015). Each receptor that recognizes the nanoparticle will induce a specific internalization mechanism and may evoke a different immunological response, which can explain at least in part the differences on the

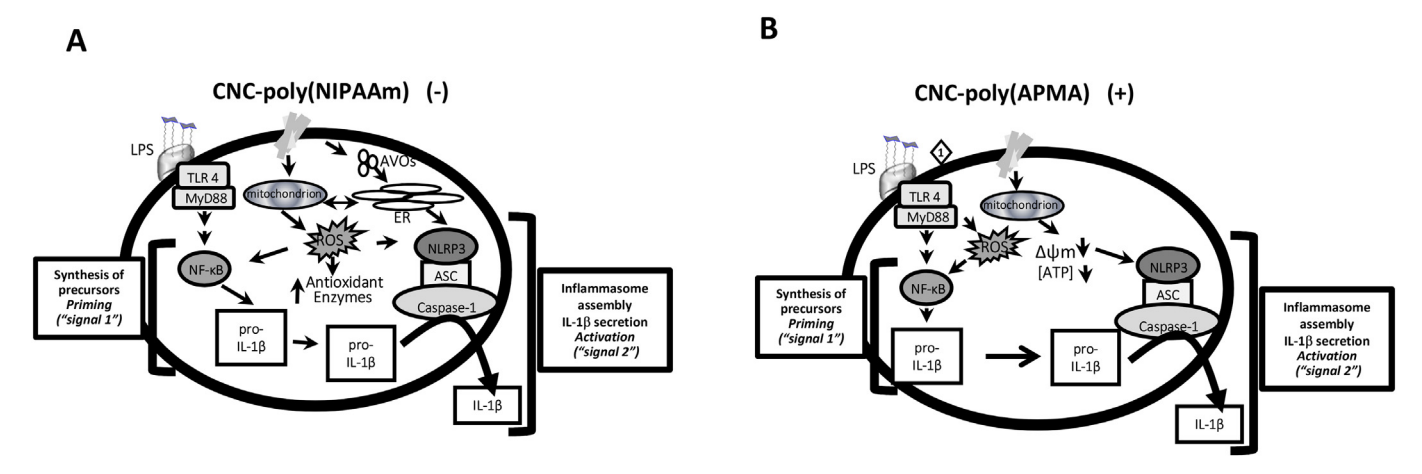


Fig. 8. Proposed mechanisms by which functionalized CNCs exert their immune responses. (A) The anionic CNCs-poly(NIPAAm) induces in greater extension the formation of acidic vesicles organelles (AVOs) which can cause an ER stress response and mitochondrial-ROS, which could contribute at least in part to the increases on the IL-1 $\beta$  secretion. In addition, CNCs-poly(NIPAAm) also induced TNF- $\alpha$  secretion in non-stimulated PMBCs, by an unknown mechanism (not depicted in this picture). (B) The cationic CNCs-poly(APMA) mainly affect mitochondrial function by disturbing membrane polarization and decreasing intracellular ATP, which could contribute for the greater effect on the NLRP3 inflammasome activation and IL-1 $\beta$  secretion.

immunological and phagocytic responses evoke by CNCs-poly(APMA) and CNCs-poly(NIPAAm). For instance, polyanionic charged nanoparticles can interact with scavengers receptor which contain collagen positive domains (Chao et al., 2013) and this receptor is associated with phagocytosis as well as pattern-associated recognition receptors (PRRs) (Gustafson et al., 2015), which are linked with NLRP3 inflammasome activation and IL1- $\beta$  secretion.

In conclusion, it appeared that the anionic CNCs-poly(NIPAAm) exerts its wider immunological effects partly via lysosomal acidification and tentative phagocytosis and potentially affecting ER homeostasis (Fig. 8A), whereas the cationic CNCs-poly(APMA) caused an immune response in LPS-stimulated cells mainly in a NLRP3-dependent manner (Fig. 8B).

#### **Funding**

This material is based upon work supported by the National Science Foundation under Grant No 1703890. This work was also partly supported by the Department of Chemistry at SUNY Plattsburgh as well as SUNY Plattsburgh Presidential Research Award 2017–2018. The authors have no conflict of interest.

#### References

Aderem, A., Underhill, D.M., 1999. Mechanisms of phagocytosis in macrophages. Annu. Rev. Immunol. 17, 593–623.

Afonina, I.S., Muller, C., Martin, S.J., Beyaert, R., 2015. Proteolytic processing of inter-leukin-1 family cytokines: variations on a common theme. Immunity 42, 991–1004.
 Arner, E.S., 2009. Focus on mammalian thioredoxin reductases-important selenoproteins with versatile functions. Biochim. Biophys. Acta 1790, 495–526.

Birben, E., Sahiner, U.M., Sackesen, C., Ezzurum, S., Kalayci, O., 2012. Oxidative stress and antioxidant defense. World Allergy Organ J 5, 9–19.

Brookes, P.S., Yoon, Y., Robotham, J.L., Anders, M.W., Sheu, S.S., 2004. Calcium, ATP, and ROS: a mitochondrial love-hate triangle. Am J Physiol Cell Physiol 287 p. C817-33, Zorov DB, Juhaszova M, and Sollott SJ, Mitochondrial reactive oxygen species (ROS) and ROS-induced ROS release. Physiol Rev, 2014. 94: p. 909-50.

Candas, D., Li, J.J., 2014. MnSOD in oxidative stress response-potential regulation via mitochondrial protein influx. Antioxid. Redox Signal. 20, 1599–1617.

Cao, Y., Long, J., Liu, L., He, T., Jiang, L., Zhao, C., et al., 2017. A review of endoplasmic reticulum (ER) stress and nanoparticle (NP) exposure. Life Sciences Vol. 186, 33–42.
 Catalan, J., Ilves, M., Jarventaus, H., Hannukainen, K.S., Kontturi, E., Vanhala, E., et al., 2015. Genotoxic and immunotoxic effects of cellulose nanocrystals in vitro. Environ. Mol. Mutagen. 56, 171–182.

Chao, Y., Karmali, P.P., Mukthavaram, R., Kesari, S., Kouznetsova, V.L., Tsigelny, I.F., et al., 2013. Direct recognition of superparamagnetic nanocrystals by macrophage scavenger receptor SR-AI. ACS Nano (7), 4289–4298.

Dimroth, P., Kaim, G., Matthey, U., 2000. Crucial role of the membrane potential for ATP synthesis by F(1)F(o) ATP synthases. J. Exp. Biol. 203, 51–59.

Dinarello, C.A., Cannon, J.G., Wolff, S.M., Bernheim, H.A., Beutler, B., Cerami, A., et al.,

1986. Tumor necrosis factor (cachectin) is an endogenous pyrogen and induces production of interleukin 1. J. Exp. Med. 163, 1433–1450.

Dobrovolskaia, M.A., 2015. Pre-clinical immunotoxicity studies of nanotechnology-for-mulated drugs: challenges, considerations and strategy. J. Control. Release 220, 571–583

Endes, C., Mueller, S., Kinnear, C., Vanhecke, D., Foster, E.J., Petri-Fink, A., et al., 2015.
Fate of cellulose nanocrystal aerosols deposited on the lung cell surface in vitro.
Biomacromolecules 16, 1267–1275.

Endes, C., Camarero-Espinosa, S., Mueller, S., Foster, E.J., Petri-Fink, A., Rothen-Rutishauser, B., et al., 2016. A critical review of the current knowledge regarding the biological impact of nanocellulose. J. Nanobiotechnol. 14, 78.

Franchi, L., Eigenbrod, T., Nunez, G., 2009. Cutting edge: TNF-alpha mediates sensitization to ATP and silica via the NLRP3 inflammasome in the absence of microbial stimulation. J. Immunol. 183, 792–796.

Guglielmo, A., Sabra, A., Elbery, M., Cerveira, M.M., Ghenov, F., Sunasee, R., et al., 2017. A mechanistic insight into curcumin modulation of the IL-1beta secretion and NLRP3 S-glutathionylation induced by needle-like cationic cellulose nanocrystals in myeloid cells. Chem. Biol. Interact. 274, 1–12.

Gustafson, H.H., Holt-Casper, D., Grainger, D.W., Ghandehari, H., 2015. Nanoparticle Uptake: The Phagocyte Problem. Nano Today 10, 487–510.

Habibi, Y., Lucia, L.A., Oj, Rojas, 2010. Cellulose nanocrystals: chemistry, self-assembly, and applications. Chem. Rev. 110, 3479–3500.

Hemraz, U.D., Lu, A., Sunasee, R., Boluk, Y., 2014. Structure of poly(N-iso-propylacrylamide) brushes and steric stability of their grafted cellulose nanocrystal dispersions. J. Colloid Interface Sci. 430, 157–165.

Hoyer-Hansen, M., Jaattela, M., 2007. Connecting endoplasmic reticulum stress to autophagy by unfolded protein response and calcium. Cell Death and Differentiation Vol. 14, 1576–1582.

Jabaut, J., Ather, J.L., Taracanova, A., Poynter, M.E., Ckless, K., 2013. Mitochondriatargeted drugs enhance Nlrp3 inflammasome-dependent IL-1beta secretion in association with alterations in cellular redox and energy status. Free Radic. Biol. Med. 60, 233–245.

Jimenez, A.S., Jaramillo, F., Hemraz, U.D., Boluk, Y., Ckless, K., Sunasee, R., 2017. Effect of surface organic coatings of cellulose nanocrystals on the viability of mammalian cell lines. Nanotechnol. Sci. Appl. 10, 123–136.

Johnston, H., Brown, D., Kermanizadeh, A., Gubbins, E., Stone, V., 2012. Investigating the relationship between nanomaterial hazard and physicochemical properties: Informing the exploitation of nanomaterials within therapeutic and diagnostic applications. J. Control. Release 164, 307–313.

Kalia, Susheel, Dufresne, Alain, Mathew Cherian, Bibin, Kaith, B.S., Avérous, Luc, Njuguna, James, et al., 2011. Cellulose-based Bio- and Nanocomposites: a Review. International Journal of Polymer Science 2011, 35.

Lebovitz, C.B., Bortnik, S.B., Sm, Gorski, 2012. Here, there be dragons: charting autophagy-related alterations in human tumors. Clin. Cancer Res. 18, 1214–1226.

Li, X., Fang, P., Mai, J., Choi, E.T., Wang, H., Xf, Yang, 2013. Targeting mitochondrial reactive oxygen species as novel therapy for inflammatory diseases and cancers. J. Hematol. Oncol. (6), 19.

Liberman, E.A., Topaly, V.P., Tsofina, L.M., Jasaitis, A.A., Skulachev, V.P., 1969. Mechanism of coupling of oxidative phosphorylation and the membrane potential of mitochondria. Nature 222, 1076–1078 Mitchell P, Coupling of phosphorylation to electron and hydrogen transfer by a chemi-osmotic type of mechanism. Nature, 1961. 191: p. 144–8.

Lunov, O., Syrovets, T., Loos, C., Nienhaus, G.U., Mailander, V., Landfester, K., et al., 2011. Amino-functionalized polystyrene nanoparticles activate the NLRP3 inflammasome in human macrophages. ACS Nano 5, 9648–9657.

Malugin, A., Ghandehari, H., 2011. Caspase 3 independent cell death induced by amorphous silica nanoparticles. Nanoscience and Nanotechnology Letters Vol. 3, 309–313.

H.W. Despres et al.

- Matsui, H., Ito, T., Ohnishi, S., 1983. Phagocytosis by macrophages. III. Effects of heatlabile opsonin and poly(L-lysine). J. Cell Sci. 59, 133–143.
- Menas, A.L., Yanamala, N., Farcas, M.T., Russo, M., Friend, S., Fournier, P.M., et al., 2017. Fibrillar vs crystalline nanocellulose pulmonary epithelial cell responses: Cytotoxicity or inflammation? Chemosphere Vol. 171, 671–680.
- Mindell, J.A., 2012. Lysosomal acidification mechanisms. Annu. Rev. Physiol. 74, 69–86.
  Mizushima, N., Yoshimori, T., Levine, B., 2010. Methods in mammalian autophagy research. Cell 140, 313–326.
- Nomura, J., So, A., Tamura, M., Busso, N., 2015. Intracellular ATP decrease mediates NLRP3 inflammasome activation upon nigericin and crystal stimulation. J. Immunol. 195, 5718–5724.
- Oslowski, C.M., Urano, F., 2011. Measuring ER stress and the unfolded protein response using mammalian tissue culture system. Methods Enzymol. 490, 71–92.
- Owens III, D.E., Peppas, N.A., 2006. Opsonization, biodistribution, and pharmacokinetics of polymeric nanoparticles. Int. J. Pharm. 307, 93–102.
- Pellegrini, C., Antonioli, L., Lopez-Castejon, G., Blandizzi, C., Fornai, M., 2017. Canonical and Non-Canonical Activation of NLRP3 Inflammasome at the Crossroad between Immune Tolerance and Intestinal Inflammation. Front. Immunol. 8, 36.
- Steinman, R.M., Mellman, I.S., Muller, W.A., Za, Cohn, 1983. Endocytosis and the recycling of plasma membrane. J. Cell Biol. 96, 1–27.
- Sunasee, R., Hemraz, U.D., 2018. Synthetic strategies for the fabrication of cationic

- surface-modified cellulose nanocrystals. Fibres Vol. 6, 15.
- Sunasee, R., Araoye, E., Pyram, D., Hemraz, U.D., Boluk, Y., Ckless, K., 2015. Cellulose nanocrystal cationic derivative induces NLRP3 inflammasome-dependent IL-1β secretion associated with mitochondrial ROS production. Biochemistry and Biophysics Reports 4, 1–9.
- Sunasee, R., Hemraz, U.D., Ckless, K., 2016. Cellulose nanocrystals: a versatile nanoplatform for emerging biomedical applications. Expert Opin Drug Deliv 13, 1243–1256.
- Tesei, A., Cortesi, M., Zamagni, A., Arienti, C., Pignatta, S., Zanoni, M., et al., 2018. Sigma receptors as endoplasmic reticulum stress "gatekeepers" and their modulators as emerging new weapons in the fight against cancer. Front. Pharmacol. 9, 711.
- Thome, M.P., Filippi-Chiela, E.C., Villodre, E.S., Migliavaca, C.B., Onzi, G.R., Felipe, K.B., et al., 2016. Ratiometric analysis of acridine orange staining in the study of acidic organelles and autophagy. J. Cell Sci. 129, 4622–4632.
- Wilson, N.S., Duewell, P., Yang, B., Li, Y., Marsters, S., Koernig, S., et al., 2014. Inflammasome-dependent and -independent IL-18 production mediates immunity to the ISCOMATRIX adjuvant. J. Immunol. 192, 3259–3268.
- Zhang, X., Zhang, H., Liang, X., Zhang, J., Tao, W., Zhu, X., et al., 2016. Iron oxide nanoparticles induce autophagosome accumulation through multiple mechanisms: lysosome impairment, mitochondrial damage, and ER stress. Mol. Pharm. 13, 2578–2587